



Timescales of AMOC decline in response to fresh water forcing

Laura C. Jackson¹ · Richard A. Wood¹

Received: 17 February 2017 / Accepted: 8 October 2017 / Published online: 13 December 2017
© Crown Copyright 2017

Abstract

The Atlantic meridional overturning circulation (AMOC) is predicted to weaken over the coming century due to warming from greenhouse gases and increased input of fresh water into the North Atlantic, however there is considerable uncertainty as to the amount and rate of AMOC weakening. Understanding what controls the rate and timescale of AMOC weakening may help to reduce this uncertainty and hence reduce the uncertainty surrounding associated impacts. As a first step towards this we consider the timescales associated with weakening in response to idealized freshening scenarios. Here we explore timescales of AMOC weakening in response to a freshening of the North Atlantic in a suite of experiments with an eddy-permitting global climate model (GCM). When the rate of fresh water added to the North Atlantic is small (0.1 Sv; 1 Sv = 1×10^6 m³/s), the timescale of AMOC weakening depends mainly on the rate of fresh water input itself and can be longer than a century. When the rate of fresh water added is large (≥ 0.3 Sv) however, the timescale is a few decades and is insensitive to the actual rate of fresh water input. This insensitivity is because with a greater rate of fresh water input the advective feedbacks become more important at exporting fresh anomalies, so the rate of freshening is similar. We find advective feedbacks from: an export of fresh anomalies by the mean flow; less volume import through the Bering Strait; a weakening AMOC transporting less subtropical water northwards; and anomalous subtropical circulations which amplify export of the fresh anomalies. This latter circulation change is driven itself by the presence of fresh anomalies exported from the subpolar gyre through geostrophy. This feedback has not been identified in previous model studies and when the rate of freshening is strong it is found to dominate the total export of fresh anomalies, and hence the timescale of AMOC decline. Although results may be model dependent, qualitatively similar mechanisms are also found in a single experiment with a different GCM.

Keywords AMOC · Timescale · Climate

1 Introduction

The Atlantic meridional overturning circulation (AMOC) is projected to decline as concentrations of greenhouse gases increase, however there is a wide range in the magnitude and speed of this decline across Global Climate Models (GCMs), leading to significant uncertainties in projections. Reintges et al. (2016) attributed the model spread in response of the AMOC to the model spread in density, and particularly salinity, changes. These model projections also generally do not include additional fresh water input into the high latitudes from melting glaciers and ice sheets, another process which can inhibit deep convection in the

North Atlantic and weaken the AMOC. Although experiments which do include realistic estimates of future fresh water input only show a small additional AMOC weakening over the next century (Swingedouw et al. 2015; Bakker et al. 2016), there are suggestions that the AMOC in the real world might be more sensitive. One line of evidence comes from paleo data showing large, rapid (over decades) changes in surface temperature which have been suggested to originate from large shifts in the AMOC in response to the addition of fresh water (McManus et al. 2004; Rahmstorf 2002; Clement and Peterson 2008). Theories suggest that the AMOC might have both stable on and off states dependent on the fresh water added to the North Atlantic (Rahmstorf 1996). Rapid transitions between such states could result in large shifts in surface temperatures such as those measured in paleo records. Studies have suggested that GCMs may be too stable since they are unable to correctly

✉ Laura C. Jackson
laura.jackson@metoffice.gov.uk

¹ Met Office Hadley Centre, Exeter, UK

simulate these large paleo changes (Valdes 2011), and that biases in GCMs associated with the transport of fresh water could affect the stability and response of the AMOC (Jackson 2013; Liu et al. 2013, 2017). Other evidence that the AMOC is potentially more sensitive in the real world than in models is recent evidence that the interannual AMOC variability in GCMs is weaker than that observed (Roberts et al. 2014). This suggests that the AMOC may be more sensitive to interannual atmospheric forcing in the real world than in models, with the implication of potentially greater sensitivity to other forcings.

Many studies have examined the question of AMOC stability using theoretical models (Rahmstorf 1996; Cimatoribus et al. 2014), Earth system models of intermediate complexity (Rahmstorf et al. 2005; Hofmann and Rahmstorf 2009) and fully coupled GCMs (Hawkins et al. 2011; Liu et al. 2013), although there are limitations for the latter in the experiments that are possible. In terms of policy however, the question of the stability of the AMOC may be less relevant than the questions of whether it is possible to detect that a threshold has been passed, the timescales and rate of AMOC decline, and whether the decline is reversible. We focus here on the question of what controls the timescale and speed of AMOC decline when fresh water is added to the Atlantic. Although warming from increased greenhouse gases undoubtedly plays a significant role in the projected weakening of the AMOC, we initially concentrate on fresh water forcing since it is believed to potentially be important for rapid changes of the AMOC. We note that these results are also relevant for understanding large, rapid paleoclimate changes that are believed to have been caused by rapid changes in the AMOC in response to large inputs of fresh water (McManus et al. 2004; Rahmstorf 2002). The scenarios applied here are idealized with large inputs of fresh water, in order to identify the signals and mechanisms. This is a first step towards understanding the response and timescales in more realistic projections. It is also likely that the timescale is sensitive to the region of fresh water input, as well as being model dependent. Hence we focus on the different mechanisms of AMOC weakening and how these affect the timescale. Little previous work has concentrated on what controls the timescale of AMOC decline. One study (Sgubin et al. 2015) considered the AMOC recovery after an increase and then decrease of greenhouse gases and related the different AMOC recoveries in different models to different inertial timescales in the recovery of salinity because of different advective responses.

Other studies have examined the response of the AMOC to idealized formulations (Stouffer et al. 2006; Swingedouw et al. 2013) or projections (Driesschaert et al. 2007; Hu et al. 2011; Bakker et al. 2016) of future fresh water input in the North Atlantic. Conclusions have been that expected fresh water input from Greenland Ice Sheets would cause little

additional AMOC weakening up to 2100, however Bakker et al. (2016) suggested that the impacts would be much larger by 2300, with an additional 37% AMOC weakening predicted in a high end scenario. Various processes have been found to affect the fate of the fresh water added, and hence the AMOC weakening. Swingedouw et al. (2013) found that the magnitude of AMOC weakening depended on the leakage of fresh anomalies from the subpolar to subtropical gyres, and that models with more asymmetric fronts between the subpolar and subtropical gyres had less export of fresh anomalies and weakened more. Hu et al. (2011) found that the hosing weakened the import of Pacific water through the Bering Strait, offsetting some of the freshening, and other studies have also found that changes in meridional fresh water transport can oppose freshening from hosing (Jackson 2013; den Toom et al. 2014). The ocean response has also been shown to be sensitive to the ocean resolution and presence of eddies (Weijer et al. 2012; den Toom et al. 2014).

In Sect. 2 we describe the model and outline the experiments. In Sect. 3 we analyze the AMOC decline and the mechanisms controlling that decline in the different experiments. The timescale over which the AMOC weakens is evaluated in Sect. 4, as well as how the mechanisms affect this timescale. A summary and conclusions are then presented in Sect. 5.

2 Methods

We use HadGEM3-GC2 which is an eddy-permitting GCM (Williams et al. 2015) that has been developed since the 5th Coupled Model Intercomparison Project (CMIP5). The GCM consists of ocean, atmosphere, land and sea-ice components. This ocean model component uses the Global Ocean version 5 (GO5) (Megann et al. 2014) of the ORCA025 configuration of the Nucleus for European Modelling of the Ocean (NEMO) (Madec 2008) which has a nominal resolution of 0.25° and 75 vertical levels. Because of the increased horizontal resolution the model does not use the GM (Gent and McWilliams 1990) parameterization for eddy mixing, however other mixing parameterizations are used including: lateral mixing along isoneutral surfaces, diapycnal mixing from a turbulent kinetic energy scheme and a background vertical eddy diffusivity (Megann et al. 2014). The model uses a linear free surface approximation which means that there is no volume change from precipitation and that freshening from surface fluxes is then represented as described in Roulet and Madec (2000). The atmosphere model is the Global Atmosphere version 6 (GA6.0) of the Met Office Unified Model, and is used with a horizontal resolution of about 60 km in mid-latitudes, and 85 levels in the vertical.

A simulation with steady preindustrial forcing provided the control, and a set of experiments were conducted where fresh water was added to the North Atlantic to drive a weakening of the AMOC. For this study we use 200 years of control; the AMOC strength is 14.5 Sv with a standard deviation of 0.9 Sv and a small upwards trend of 0.27 Sv per century. A previous study (Mecking et al. 2016) showed that the addition of a large amount of fresh water into the North Atlantic in HadGEM3-GC2 caused the AMOC to substantially weaken, with no recovery found over the subsequent centuries. Instead of adding a large amount of fresh water over a decade, as in that study, we use the more standard methodology of applying an additional fresh water flux to the surface ocean (hosing). We use an idealized forcing with the flux applied uniformly over the Arctic and North Atlantic north of 50° N. To prevent the hosing changing the global mean salinity, we also apply a volume compensation for the hosing by removing fresh water from each grid cell through the ocean volume. The amount to be removed is calculated so that the global volume average salinity change from the hosing and compensation is zero. We apply several rates of hosing (0.1, 0.2, 0.3, 0.5, 0.7, 1.0 Sv, where 1 Sverdrup = 10⁶m³/s) for 150–250 years. Experiment names and details are shown in Table 1.

A comparison is also made in Sect. 3.4 with results from a hosing experiment with a different GCM, HadCM3 (Gordon et al. 2000). This is an earlier coupled GCM with lower resolution (1.25° and 20 vertical layers in the ocean). Although both models were developed at the Met Office Hadley Centre, all components use very different models, with the ocean and sea ice components having a different provenance. The HadCM3 experiment used for the comparison (referred to here as hadcm3_hos10) also applies 1 Sv hosing to the North Atlantic (over 50–70°N rather than including the Arctic as well). Further details of the model and experiment can be found in Jackson (2013) (where HadCM3 is the unfluxadjusted model).

AMOC timeseries are measured as the maximum of the streamfunction over 200–3000 m at 26.5 N. Details of the salinity budget can be found in Appendix and a description of the numerical calculation in 6.3.

2.1 Piecewise linear function

In Sect. 4 we fit timeseries with a piecewise linear function. This is a function with two linear segments and a join at time T . Firstly we choose a point τ in the timeseries and fit the timeseries up to that point with a linear function using least squares regression (giving a trend and an intercept). We then fit the timeseries after τ in the same way, but with the constraint that the value at time τ matches that from the first line. This gives us a second trend. We then repeat this for all possible values of τ in the timeseries and choose the value of $\tau = T$ that minimizes the root mean square error of the function from the timeseries data.

3 Mechanism of AMOC response

3.1 The AMOC

In the preindustrial control the AMOC consists of a coherent overturning cell in the top 2500 m of the Atlantic, with a strength of 14.5 Sv. This is slightly weaker than the observed value (from 2004 to 2012) of 17.2 ± 0.9 Sv (McCarthy et al. 2015) (Fig. 1).

The AMOC weakens to <4 Sv in all experiments where hosing is applied, with the reduction occurring over timescales of ~ 50–200 years. The rate and magnitude of the weakening of the 0.1 and 1 Sv hosing experiments are consistent with those found in a multi-model study (Stouffer et al. 2006). The AMOC in our experiments decreases faster with stronger hosing, however there is a saturation of this effect at higher hosing rates (with little difference in the AMOC decrease between 0.5 and 1 Sv of hosing). This suggests that, even with infinite hosing, there is a limit on how fast the AMOC can decrease. Timeseries of North Atlantic March mixed layer depth (Fig. 1b) show that deep convection decreases faster than the AMOC, and that the AMOC can continue decreasing for decades after deep convection has ceased. This will be discussed further in Sect. 4 where we investigate the timescales in more depth.

The 'off' state reached consists of a very weak AMOC cell with very little sinking in the northern hemisphere

Table 1 Experiments and the fits of a piecewise linear model to the AMOC timeseries from Fig. 11

	Hosing (Sv)	Length of run	T (year)	First trend (Sv/year)	Second trend (Sv/year)	T_{mld} (year)
hos01	0.1	250	250	-0.04		187
hos02	0.2	200	78	-0.11	-0.010	49
hos03	0.3	150	44	-0.21	-0.017	33
hos05	0.5	200	40	-0.23	-0.014	21
hos07	0.7	150	38	-0.24	-0.019	6
hos10	1.0	200	36	-0.24	-0.012	4

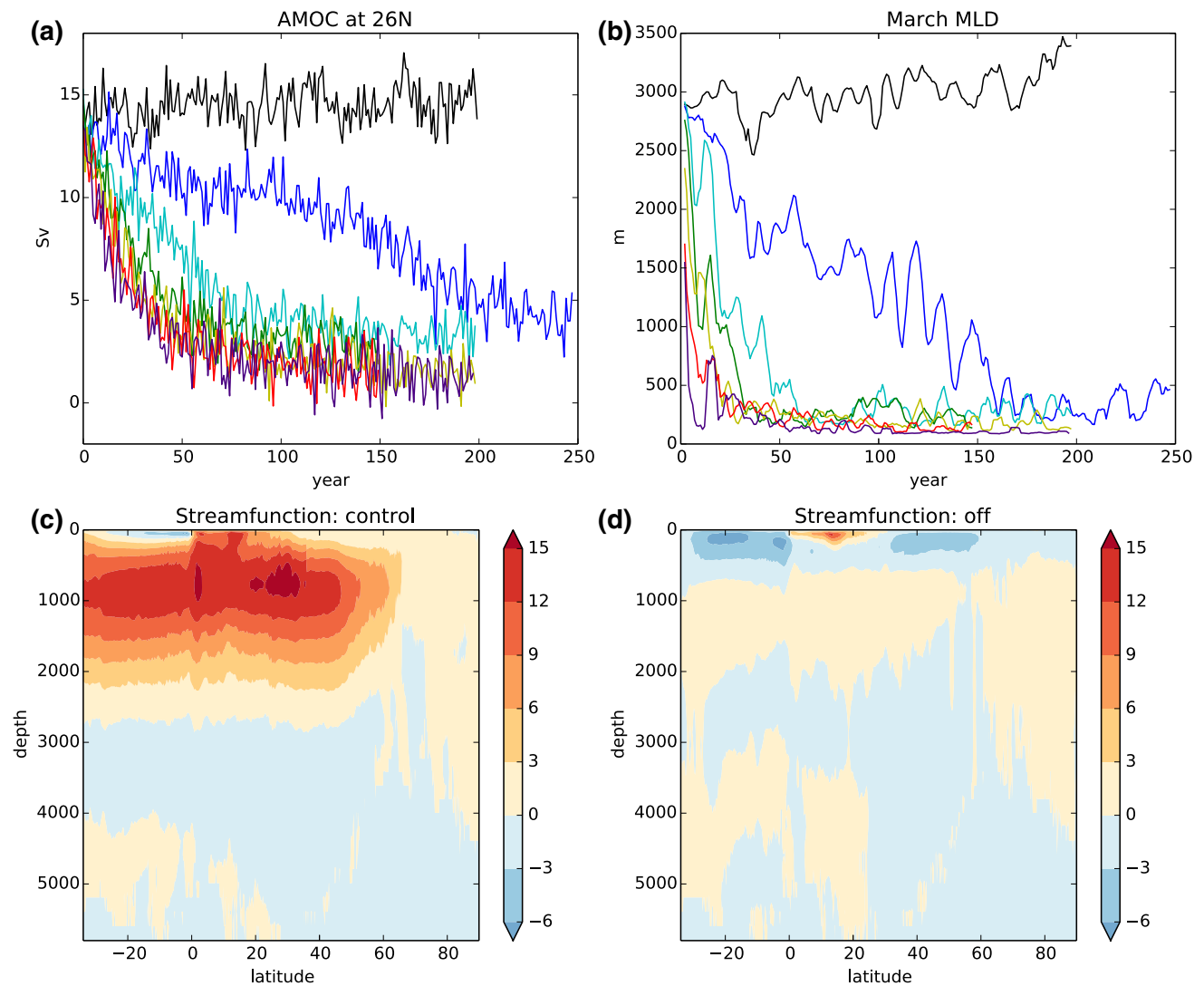


Fig. 1 AMOC. **a** Timeseries of AMOC (at 26 N) and **b** timeseries of maximum March mixed layer depth over the subpolar North Atlantic (smoothed with a 5 year running mean) for experiments hos01 (blue), hos02 (cyan), hos03 (green), hos05 (yellow), hos07 (red), hos10 (purple)

and the control (black). **c** Time mean Atlantic streamfunction from the control (years 150–200). **d** Time mean Atlantic streamfunction after strong hosing (years 150–200 of hos10)

(Fig. 1c). Some previous studies have found off states with large reversed Atlantic cells either with stronger Antarctic bottom water cells or cells associated with Antarctic intermediate water (Marotzke and Willebrand 1991; Manabe and Stouffer 1999; Gregory et al. 2003); the results in Jackson et al. (2016) suggest that the type of off state reached could influence the stability of the off state. In these experiments there is no strengthening of the deep Antarctic bottom water reverse cell, although we can see the appearance of a weak reverse cell in the upper 1000 m, which may be related to an Antarctic intermediate water cell. A similar off state was found in Mecking et al. (2016) where the same GCM was forced with a different hosing

scenario, however the off state in our experiments has a weaker AMOC cell and stronger upper ocean reverse cell.

3.2 Relationship to salinity

Many previous studies have found a strong relationship between the AMOC strength and North Atlantic density (Thorpe et al. 2001; Swingedouw et al. 2007; Jackson et al. 2016), since density changes in the subpolar North Atlantic lead to greater sinking and an acceleration of the deep western boundary currents that make up the return branch of the AMOC (Straneo 2006). In these experiments density changes are dominated by salinity changes, leading to

a strong relationship between North Atlantic salinity and the AMOC. Figure 2 shows a scatter plot of North Atlantic (between 30°N and the Bering Strait) volume averaged salinity against AMOC strength. There is a strong correlation (0.92) for salinities greater than 34.95 PSU, hence understanding of the AMOC decline may be gained by examining the salinity changes in the North Atlantic. Note that the AMOC (as measured here by the maximum value at 26.5 N) does not decrease below a background value of 0–2 Sv even when the salinities become fresher. A different metric might capture the development of a shallow reverse (negative) cell when the freshening is large (Fig. 1), however in this study we are focusing on the weakening of the positive AMOC cell.

The average salinity of the North Atlantic (\bar{S}) is affected by the addition of fresh water from the hosing flux (F_H) and by changes in advection (F_{adv}), changes in diffusion (F_D) and surface fluxes (evaporation–precipitation–runoff, F_{surf}) that occur as the climate system responds. Changes in sea ice can also affect the salinity, however these are found to be negligible in these experiments and are therefore neglected. Hence the salinity budget (see Appendix) is given by

$$v \frac{d\bar{S}}{dt} \approx -F_H + F_{adv} + F_{surf} + F_D \tag{1}$$

where v is the volume of the region which remains constant. These terms are shown in Fig. 3. In each experiment the hosing starts abruptly at the start of the experiment, so before the advection and surface fluxes respond we have $v d\bar{S}/dt = -F_H$. Over time the advective terms change to oppose the freshening from the hosing. At least part of this is the removal of fresh anomalies generated in the hosing

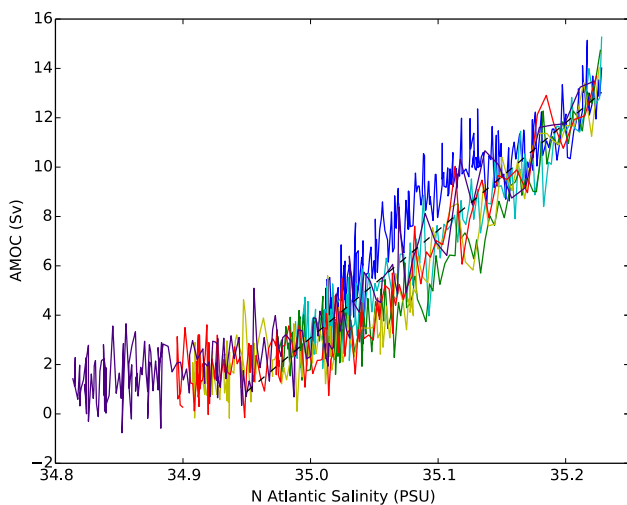


Fig. 2 Plot of AMOC strength Q against North Atlantic salinity. A linear fit to values where $S > 34.95$ PSU gives a regression slope of 43.6 Sv/PSU and a correlation coefficient of 0.93 (black dashed line). Colors are the same as in Fig. 1

region by the circulation, however there are also changes in the circulation itself which will be discussed below. There is also a slight salinification from changes in the surface fluxes caused by a reduction in net precipitation (not shown), and a slight salinification from diffusion in hos01, however most of the opposition to the freshening comes from advective changes. Eventually a balance is reached where the increased freshening from the hosing is balanced by advective and surface fluxes, and the magnitude of $d\bar{S}/dt$ is small. Note that $d\bar{S}/dt$ is still weakly negative in all experiments, implying a further gradual freshening which is consistent with the picture of a slowly weakening AMOC after the initial decline.

Over the time of AMOC decrease T (which is defined and discussed in more detail in Sect. 4) the total amount of fresh water added to the North Atlantic is TH where H is the hosing flux. We can calculate where this fresh water goes by integrating the terms in Eq. 1 over the time T ; this is shown in Fig. 4 as a percentage of the total fresh water input. When the hosing is weak, $\approx 90\%$ of fresh water goes into freshening the North Atlantic, with $\approx 10\%$ lost through changes in advection and surface fluxes each. When the hosing is stronger, the advection is more efficient at removing fresh water ($\approx 50\%$), so less fresh water is available to freshen the North Atlantic.

3.3 Response of advection

The influence of advection on the salinity of the North Atlantic can be split into 3 components (see Appendix):

$$F_{adv} = F_{thr} + F_S + F_N \tag{2}$$

where F_{thr} is the component due the volume transport through the region (throughflow) having different salinities at the boundaries. $F_N = \int_{BS} v S dx dz$ is the exchange of salinity across the northern boundary (taken to be the Bering Strait) which is found to be negligible. $F_S = \int_{30N} v S dx dz$ is the exchange of salinity across the southern boundary (30° N). Timeseries for these terms (as anomalies from the control) are shown in Fig. 5a, b for two experiments hos02 and hos10. The exchange across the southern boundary can further be decomposed into terms related to the variations of salinity and velocity separately (see Appendix):

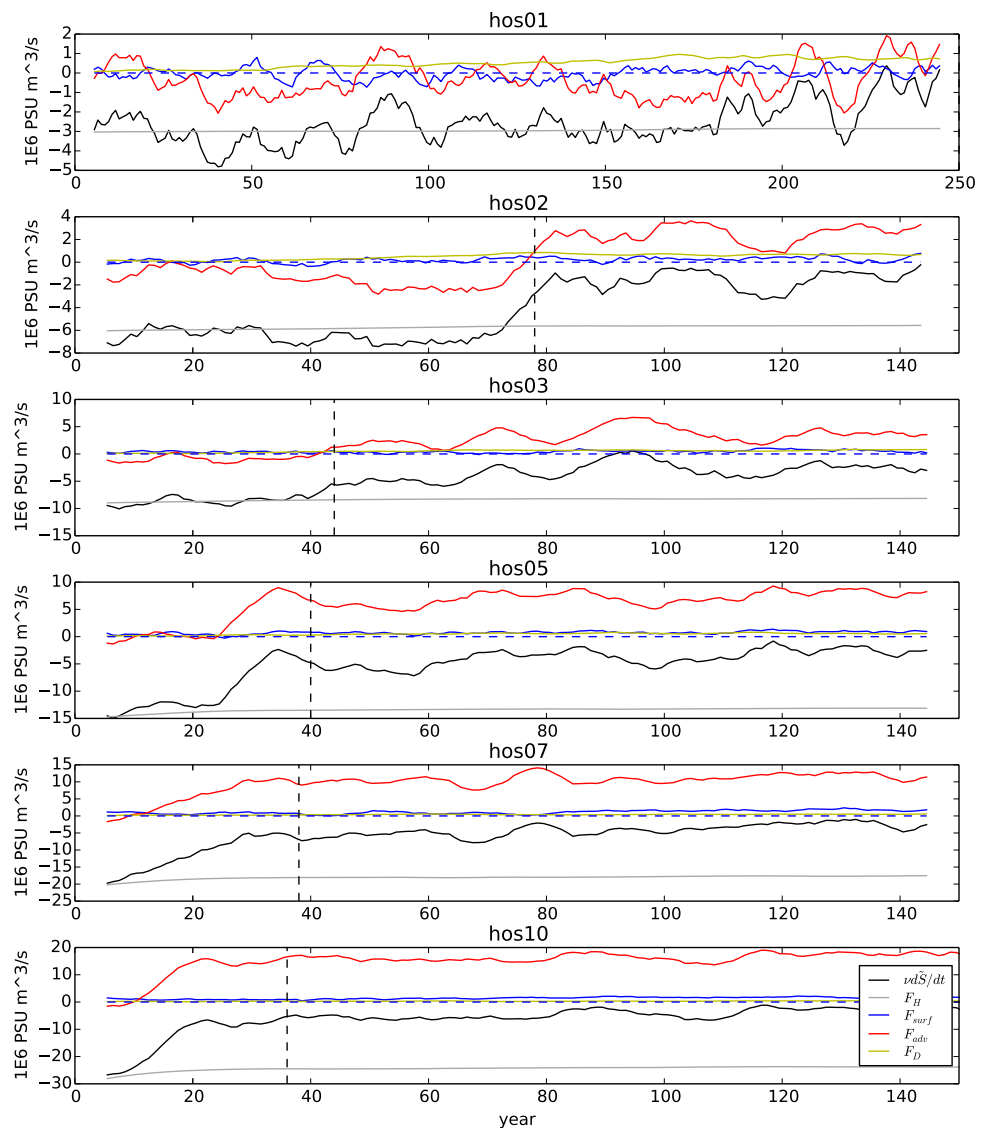
$$F_S = F_{v_e S'} + F_{v' S_c} + F_{v' S'} \tag{3}$$

Alternatively the exchange across the southern boundary can be decomposed into terms related to the overturning or gyre components (see Appendix):

$$F_S = F_o + F_g \tag{4}$$

These two decompositions are shown in Fig. 5c, d.

Fig. 3 Timeseries of terms from the salinity budget (Eq. 1) for the six hosing experiments as anomalies from the control experiment with smoothing from a 10 year running mean. Terms are: salinity tendency (vdS/dt , black), hosing $-F_H$ (gray), changes in salinity advection (red), changes in diffusion (yellow) and changes in surface fluxes (blue). The dashed vertical line shows the time T (see Table 1). Note the different time axis in the top panel. The black horizontal dashed line shows the zero line



Examination of the different components of advection reveals four processes that are contributing to the changes in advection seen in Fig. 3:

- Changes in the throughflow component cause salinification (cyan lines, Fig. 5). This is found to be because of changes in the total transport through the region (not shown), rather than changes in salinity. The volume transport through the Bering Straits weakens, and in stronger hosing cases reverses. These transport changes are likely caused by a reduction of the gradient in sea surface height between the Atlantic and Pacific basins due to the freshening of the North Atlantic.
- Fresh anomalies generated by the hosing would be exported through the south boundary if the circulation does not change, resulting in salinification (purple dotted lines, Fig. 5). This export is mostly done by

the gyre circulation (thick purple lines). Other studies have also found a salinification of the equatorial North Atlantic from a southwards shift in the Intertropical Convergence Zone (Vellinga and Wu 2004; Stouffer et al. 2006, ITCZ), providing saline anomalies to be advected northwards in the western boundary current, which would also salinify the subpolar North Atlantic. There is some low latitude and western boundary current salinification in the weaker hosing experiments (not shown), however in the strong hosing cases the recirculation of fresh anomalies in the subtropical gyre outweighs the import of saltier water from the ITCZ region. Over time this results in the freshening of the western boundary current and a reversal from an initial export of fresh anomalies to a net import of fresh anomalies (purple dotted line, Fig. 5d). This term does assume no change in the velocity, so does not take into

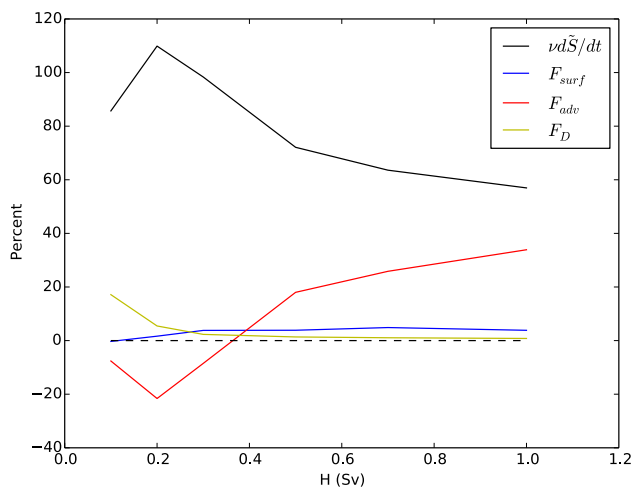


Fig. 4 Percentage of total fresh water added over the time of AMOC decline (T) which goes into changing the North Atlantic salinity (black), is removed through net changes advection (red), through diffusion (yellow) or removed through changes in surface fluxes (blue). The black dashed line shows the zero line

account the weakening of the AMOC itself. Hence the decomposition is misleading at this point.

- Changes in circulation alone cause an additional freshening (purple dashed lines, Fig. 5). This is found to be caused by the weakening of the AMOC (pale purple lines) which imports less of the saline subtropical water, and has a freshening contribution.
- There is also a large contribution from $F_{v'S'}$ in hos10 (purple dash-dot lines, Fig. 5); this is the covariance of velocity and salinity anomalies. We will show later that this is because of an anomalous circulation in the upper eastern subtropics which exports fresh anomalies generated by the hosing. Hence this term acts to offset the freshening from the hosing.

In the initial phase of AMOC weakening there are three components that act to salinify the North Atlantic and oppose the freshening from the hosing, and one component that acts to amplify the freshening. This latter component, the reduced import of saline water from a weakening AMOC is often referred to as the advective feedback. It is this feedback that is responsible for nonlinear behavior and hysteresis in simple models of the AMOC (Rahmstorf 1996; Cimatoribus et al. 2014), and has been shown to be important (when considering the advective changes into the Atlantic from the Southern Ocean) for AMOC behavior in GCMs (de Vries and Weber 2005; Jackson 2013; Liu et al. 2013). One other way in which the hosing could affect the circulation is through an input of volume locally that induces a Goldsborough-Stommel circulation (Huang and Schmitt 1993), however this would not directly affect the transport at the southern boundary which is south of the hosing region.

One question is whether the presence of eddies plays a role in the salt transport given that the model used is of eddy-permitting resolution. Mecking et al. (2016) calculated an eddy component of the transport F_S as the sub-monthly covariances of velocity and salinity (see also Appendix) for this model. They found this transport to be small, although it played a role in the budget of the tropical Atlantic. We do not find the eddy transport to be significant in the region considered here. Other studies have found eddy-driven mixing to play a role in spreading fresh anomalies from hosing (den Toom et al. 2014; Boning et al. 2016), however the impact on AMOC weakening has been mixed: Spence et al. (2012) found greater AMOC weakening at high resolution but Weijer et al. (2012) found similar magnitudes of AMOC decline at low and high resolutions.

It might be expected that when the hosing input increases, the advective changes become stronger. Inspection of the advective changes from Fig. 5 reveal that this is only partially true. While the F_{thr} and $F_{v'S'}$ both respond substantially more in hos10 than hos02, the responses from changes of velocity and salinity alone show little increase with greater hosing. For the response related to velocity changes alone, this can be understood by regarding $F_{v'Sc}$ as the transport due to the anomalous overturning circulation. Since the AMOC changes by the same amount in each experiment (reduces to near zero), the changes in this transport would be expected to be similar. The changes due to advection of salinity anomalies alone are more complex. In hos10 there is a faster response with fresh anomalies being exported earlier in the experiment, however (as discussed above) these fresh anomalies recirculate in the subtropical gyre, opposing additional freshening.

3.4 East subtropical circulation

Since the covariance of velocity and salinity anomalies ($F_{v'S'}$) plays a large role in the Atlantic salinity budget, we examine cross sections at 30°N to investigate the processes responsible for changes in this term (Fig. 6). In the control the upper waters are warm and saline with isopycnals sloping downwards towards the west. Velocities show a strong northwards velocity on the western boundary with recirculation slightly off shore. This is the northwards flow of the Gulf Stream, some of which is returned at depth, some locally recirculated, and some returned in the subtropical gyre (as seen by the southwards velocities across most of the upper 500 m). At the eastern boundary there is also an Eastern boundary current system caused by wind-driven upwelling at the boundary (Gill 1982).

In the experiments with hosing, fresh anomalies (from the addition of hosing over regions north of 50°N) are advected southwards in the subtropical gyre (see also Fig. 7). This results in a fresh and light pool of water in the eastern

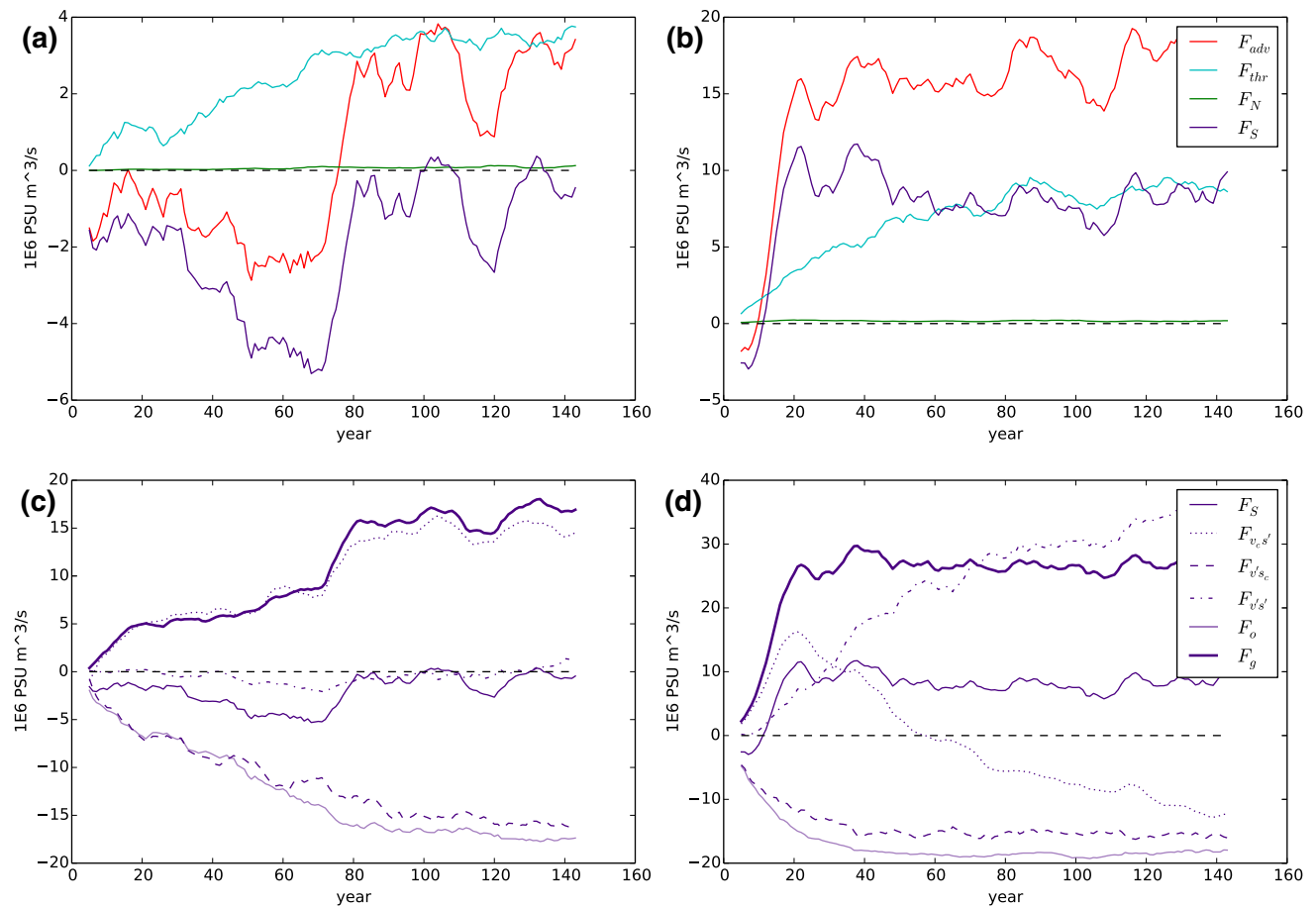


Fig. 5 Anomalous advective terms for hos02 (**a**, **c**) and hos10 (**b**, **d**). Shown are (**a**, **b**): F_{adv} (red), contributions from the throughflow transport term F_{thr} (cyan), from the exchange across the Bering Strait F_N (green) and from the exchange at 30°N F_S (purple) (see Eq. 2). In (**c**, **d**) the latter is decomposed into anomalous advection due to

salinity variations (dotted line), due to velocity variations (dashed line) and due to co-variations in velocity and salinity (dot dash). Also shown is the decomposition into overturning (pale line) and gyre (thick line) components. See Eqs. 3 and 4. The black horizontal dashed line shows the zero line

subtropical gyre (Fig. 6b, d). Velocities show a shift of the southwards gyre flow to the eastern part of the basin, and particularly in the near surface waters between $10\text{--}20^\circ\text{W}$ (see also velocity anomaly in 8).

To see where the covariance of salinity and velocity anomalies contributes to the export of fresh anomalies, we multiply the anomalous velocity and salinity fields ($F_{v's}$, Fig. 8c). There is a contribution from the Gulf Stream as the northwards flow weakens and the water freshens (as the fresh anomaly recirculates in the subtropical gyre) and a contribution from the eastern section where there is a greater southwards transport of fresher water. To assess the contributions to the total transport we do a running integral F_{vs} from the eastern boundary, and integrate over depth (Fig. 8d). A large contribution to the increased export of fresh anomalies comes from near the eastern boundary over the top 200 m. This is partly offset by the reduced export of fresh anomalies over most of the upper gyre. There is also

an increased export of fresh anomalies from the Gulf Stream weakening.

The southwards transport in the eastern section is intrinsically linked to the fresh anomaly through geostrophic balance (Fig. 8b). Hence the southwards export of fresh anomalies by the mean circulation generates anomalous geostrophic velocities which shift the southwards gyre flow to the eastern part of the basin where the water is fresher and cooler. This enhances the export of fresh anomalies. Although there is some ageostrophic contribution near the boundaries, most of the transport across the section can be explained by the geostrophic contribution to $F_{v's}$ (Fig. 8d, blue dashed line). The total southwards transport by the gyre is unchanged (consistent with Sverdrup theory (Vallis 2006) since there is no significant change in the wind stress curl). Instead there is a change in the vertical distribution of the transport resulting in greater southwards flow in the upper east part of the basing where the fresh anomalies are greatest.

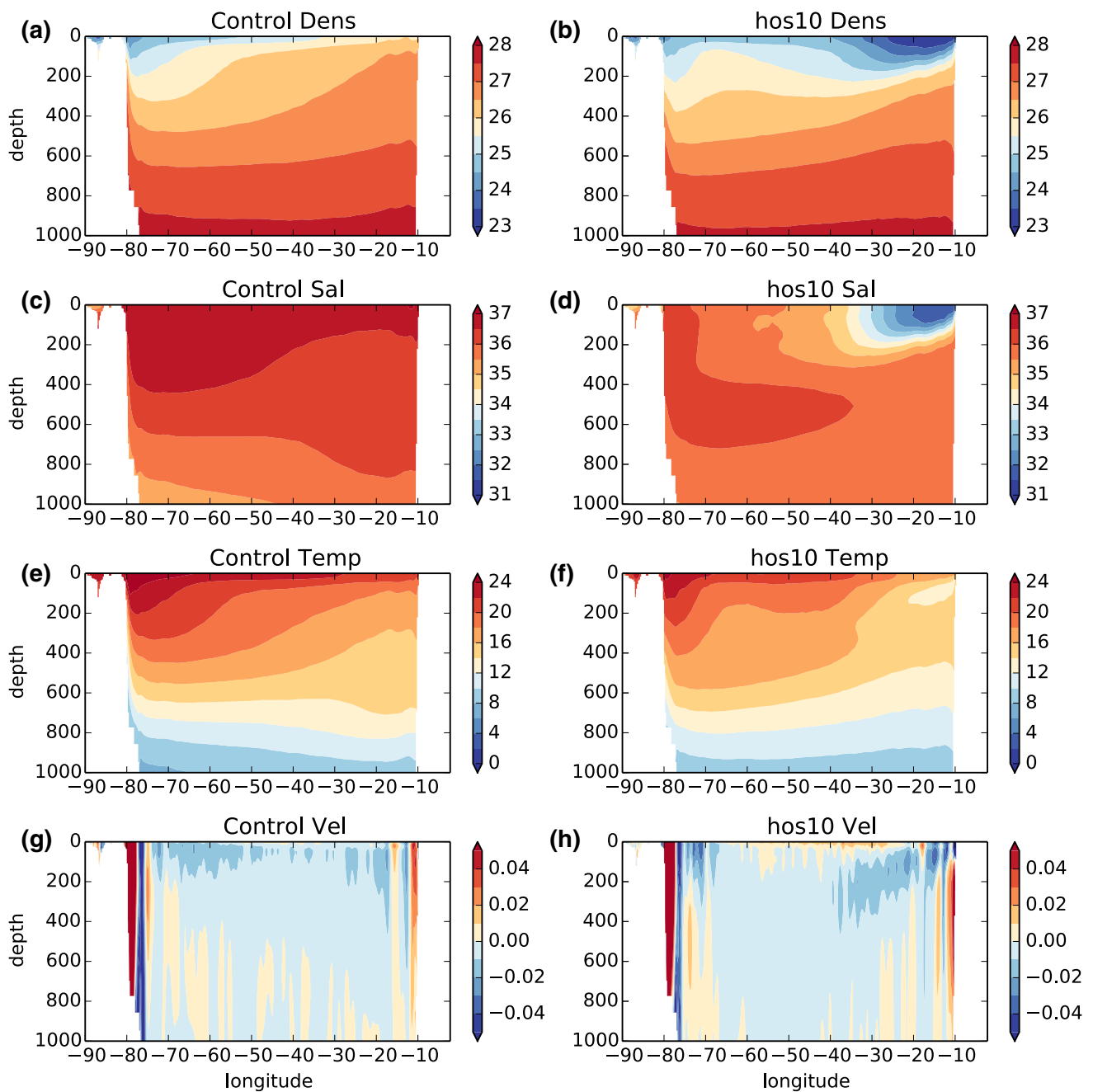


Fig. 6 Cross sections at 30°N for the control (**a, c, e, g**) and years 30–40 of hos10 (**b, d, f, h**). **a, b** Potential density (kg/m^3), **c, d** salinity (PSU), **e, f** temperature ($^{\circ}C$) and **g, h** northwards velocity (m/s)

This shift in the near surface circulation plays a greater role when the hosing is stronger because of the depth distribution of the fresh anomaly. Figure 9 shows the salinity anomaly from each experiment at a time when each experiment has experienced the same total hosing (20 Sv year) but over different lengths of time. In the experiments where the hosing is weak, although convection decreases over time, it is still able to mix the fresh water applied at the surface through the water column resulting in a fresh subpolar gyre

down to 3000 m. When the hosing is stronger, convection decreases more quickly and does not freshen the subsurface waters. Instead there is actually a slight increase in subsurface subpolar salinity. As a result the fresh water applied is confined to the surface, resulting in a very fresh surface layer which extends further south into the subtropical gyre. It is this fresh anomaly exported into the subtropics that is responsible for the near surface subtropical circulation that develops.

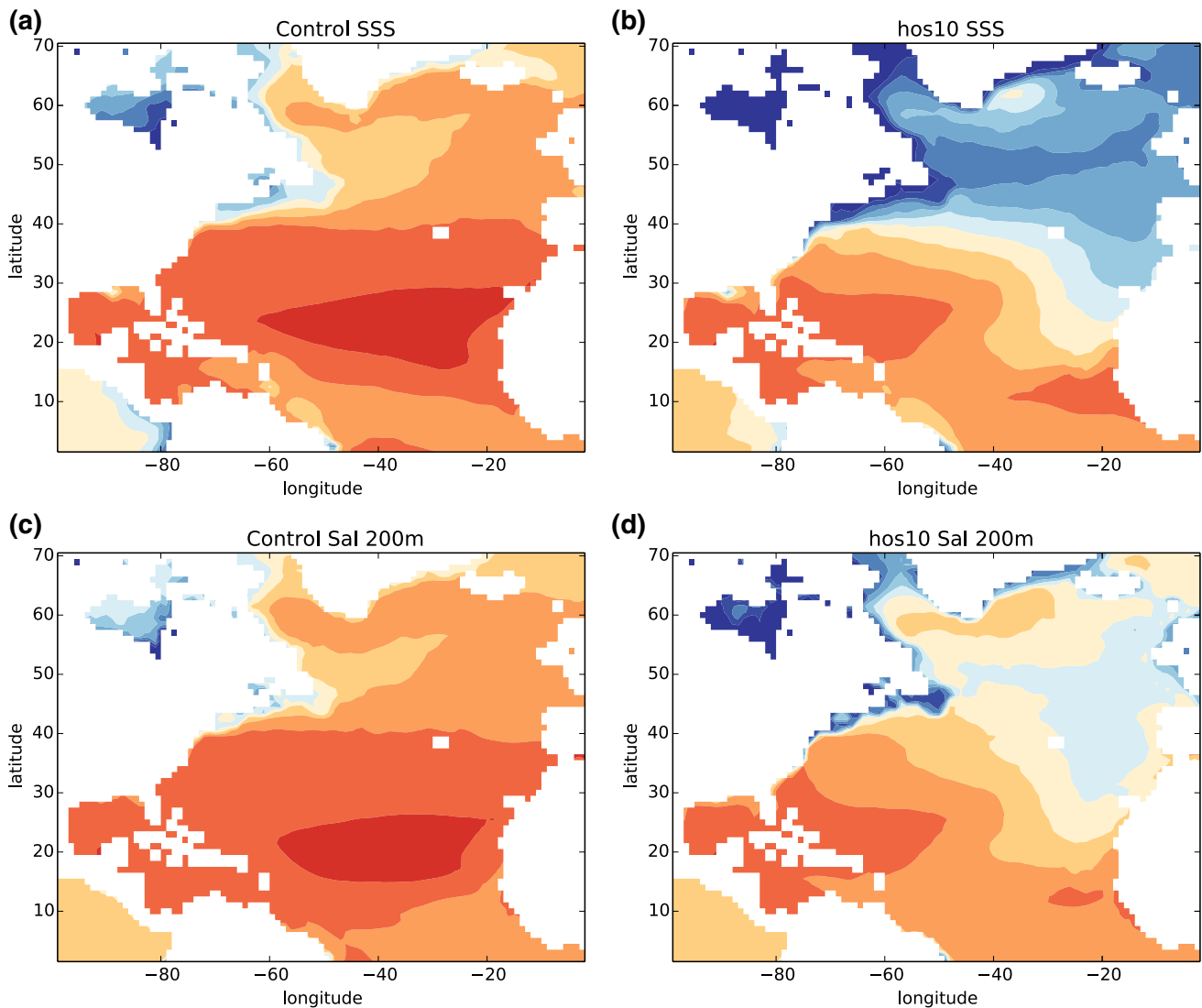


Fig. 7 Sea surface salinity (a, b) and salinity averaged over the top 200 m (c, d) for the control (a, c) and (b, d) for years 30–40 of hos10

A comparison with a similar experiment with a different GCM (hadcm3_hos10) shows a similar picture (Fig. 10). The evolution of the salinity budget terms is qualitatively similar to that in hos10, although there are differences in timing and magnitude (note that the throughflow component is zero in this model because it allows no net volume transport through the Bering Strait). It also shows similar patterns of velocity and salinity anomalies and $F_{v,s}$. Other model experiments have also shown export of fresh anomalies from the subpolar gyre through the eastern subtropical pathway in many, though not all, models (Stouffer et al. 2006). Indeed Swingedouw et al. (2013) found that models with less export of fresh anomalies through this pathway showed a great AMOC decrease, consistent with our findings. These results suggest that the shifting of this circulation and its role in exporting fresh anomalies is

likely present in other models, however its importance in the salinity budget is likely to be model dependent.

In summary, the hosing initially freshens the North Atlantic and weakens the AMOC. The weakening AMOC transports less of the saline subtropical water into the subpolar, sinking regions, exacerbating the freshening. At the same time, the throughflow transport through the North Atlantic weakens, resulting in less import of fresher Pacific water, and fresh anomalies are exported to the subtropics through the gyre circulation. This export of fresh anomalies in the eastern subtropics drives an anomalous circulation which amplifies the export of fresh anomalies. The advective changes which act to salinify the North Atlantic outweigh the freshening from the weakening AMOC, and hence the freshening from the hosing is opposed, and eventually balanced, by net changes in advection. There

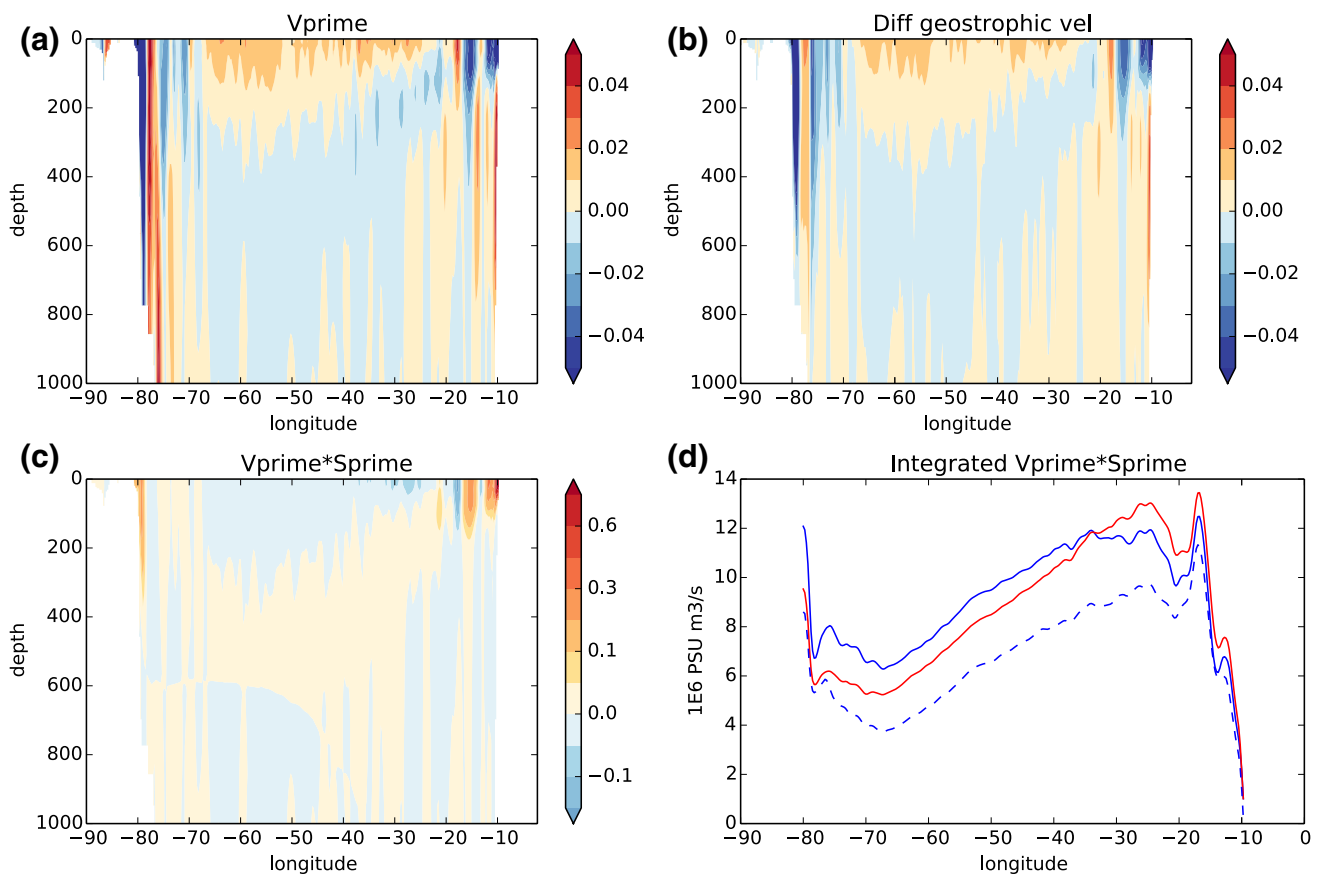


Fig. 8 Cross sections of anomalies at 30°N (from years 30–40 of hos10—control). **a** Anomalous northwards velocity (m/s), **b** geostrophic velocity implied by the anomalous density (m/s), **c** Anomalous velocity multiplied by anomalous salinity (F_{vS} , $\text{PSU}m/s$), **d** the

integral of F_{vS} from that longitude to the eastern boundary and over the total depth (blue) or top 200 m (red). Also shown is the integral of the geostrophic part of F_{vS} (blue dashed). Units are in $10^6 \text{ PSU } m^3/s$

is also a small contribution from surface fluxes which also act to oppose the hosing.

4 Timescales of decline

The AMOC decrease consists of a relatively fast initial decrease and then a slower weakening trend (Fig. 11). Fitting a piecewise linear function (see Sect. 2) gives us two trends and the change year (time at which the function changes). We define the timescale T of AMOC decline to be this change year, noting that in each experiment this is also the year at which the AMOC reaches 3–4 Sv. For the case where the hosing is 0.1 Sv, there is no clear change from fast to slow decline, so we instead define the time T to be year 250, where the AMOC has reached ≈ 4 Sv. Calculated values of T and the trends are shown in Table 1. The first trend becomes more negative as the hosing increases and the timescale T decreases reflecting a stronger and faster decline. The second trend is relatively uniform across the experiments. We also

calculate the timescale of March mixed layer depth (MLD; shown in Fig. 1b) in the same way and call this T_{mld} .

The timescales T and T_{mld} are shown in the solid lines in Fig. 12 (see also Table 1). In all experiments we find that the AMOC takes longer to decrease than the mixed layer depth ($T > T_{mld}$), and we find that both timescales vary inversely with the hosing rate, although T has little further decrease for $H > 0.3$ Sv. We would expect T and T_{mld} to be infinite when the hosing is zero (ie there is no decrease in the AMOC or MLD). Previous hosing experiments have also found that with weak hosing the AMOC can stabilize at a slightly weaker strength (Stouffer et al. 2006; Hofmann and Rahmstorf 2009). In those cases the timescale would also be infinite for non-zero hosing since the AMOC does not decrease to a small value (here ≈ 4 Sv). At the other end of the scale, the timescales show significant differences. The timescale for MLD collapse tends towards zero for large hosing rates, since a very large fresh water input could freshen the surface enough to instantaneously shut down deep convection. However the timescale for AMOC collapse appears to converge to a value T_0 of a few decades. This is because the AMOC is related to the salinity in

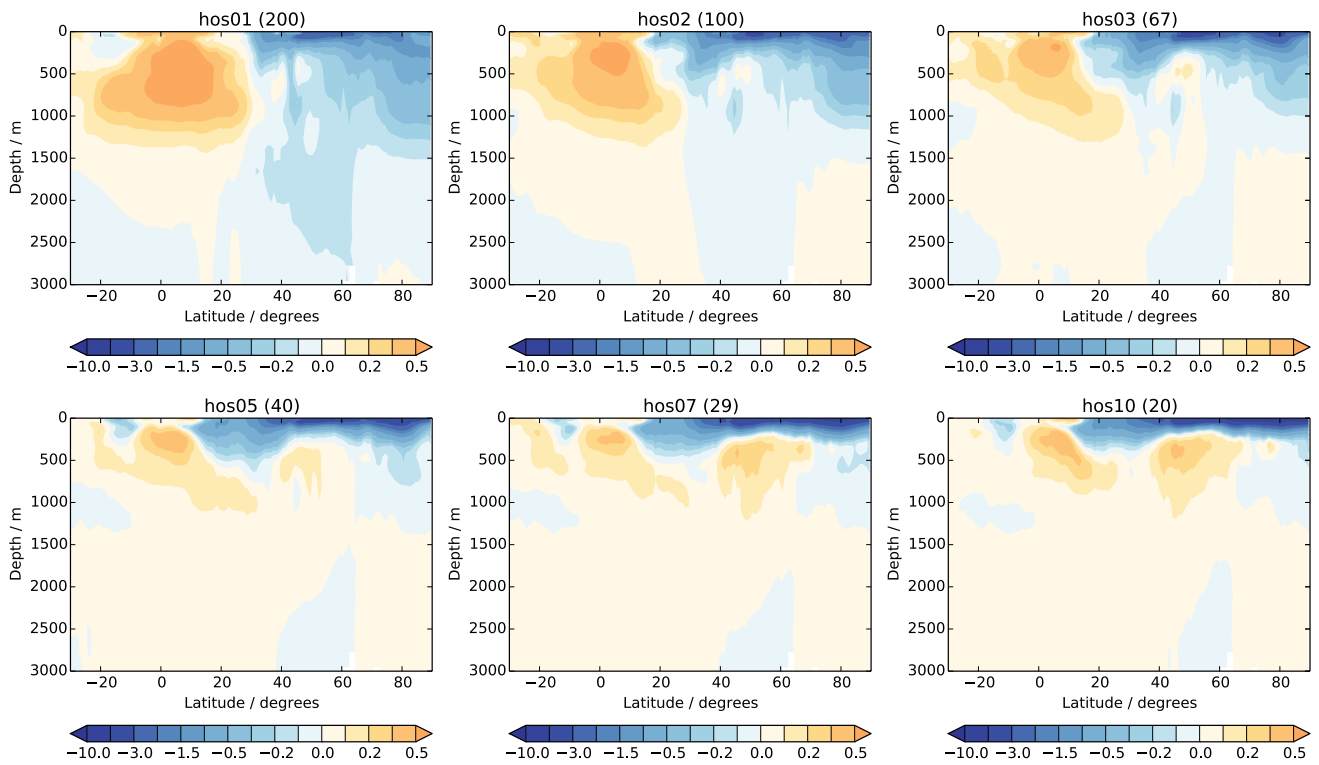


Fig. 9 Salinity anomalies averaged across the Atlantic for the six experiments. Each plot is an annual mean after 20 Sv year of hosing (year for each experiment is shown in the title)

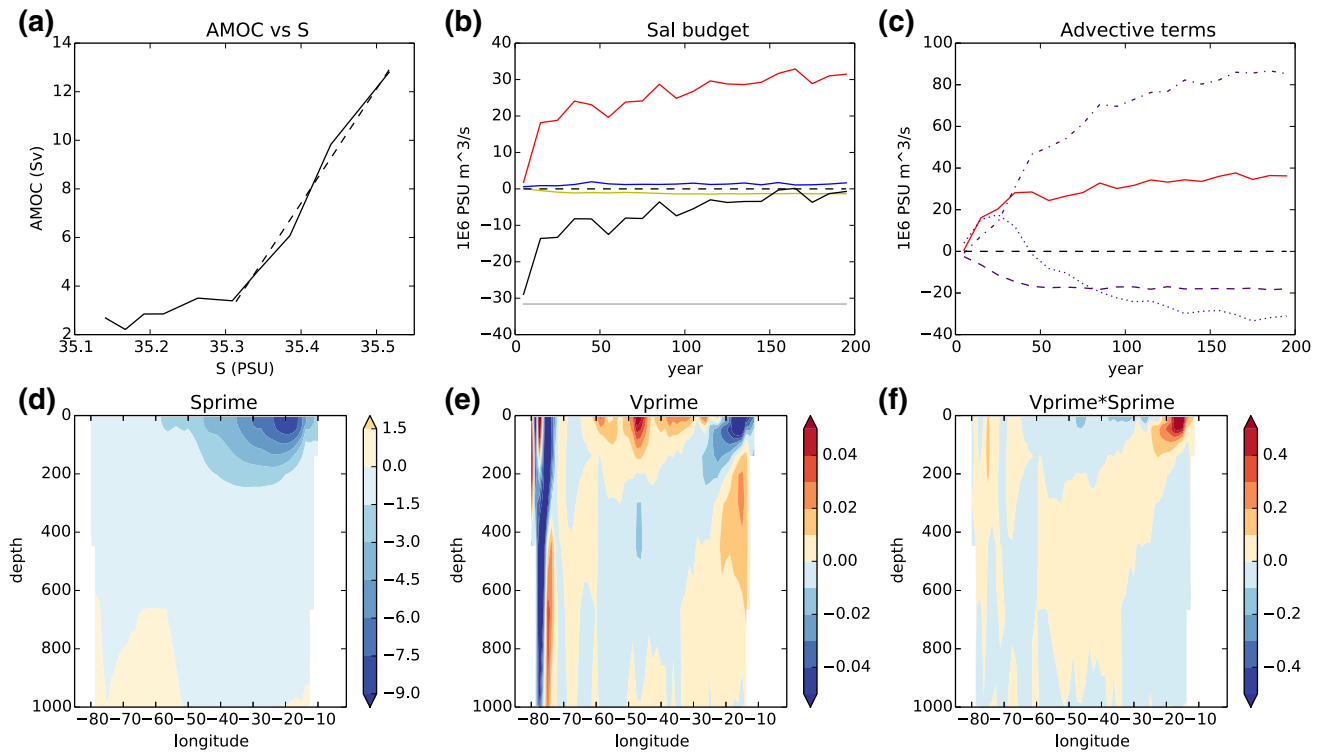


Fig. 10 Comparison with hadem3_hos10. **a** Plots of AMOC strength against Atlantic salinity as in Fig. 2. A regression over the first 50 years (shown with a dashed line) gives a slope of 47 Sv/PSU. **b** Salinity budget as in Fig. 3. **c** Advective terms as in Fig. 5. **d** Anomalous salinity at 30°N, **e** anomalous velocity at 30°N and **f** anomalous velocity multiplied by anomalous salinity (as in Fig. 8)

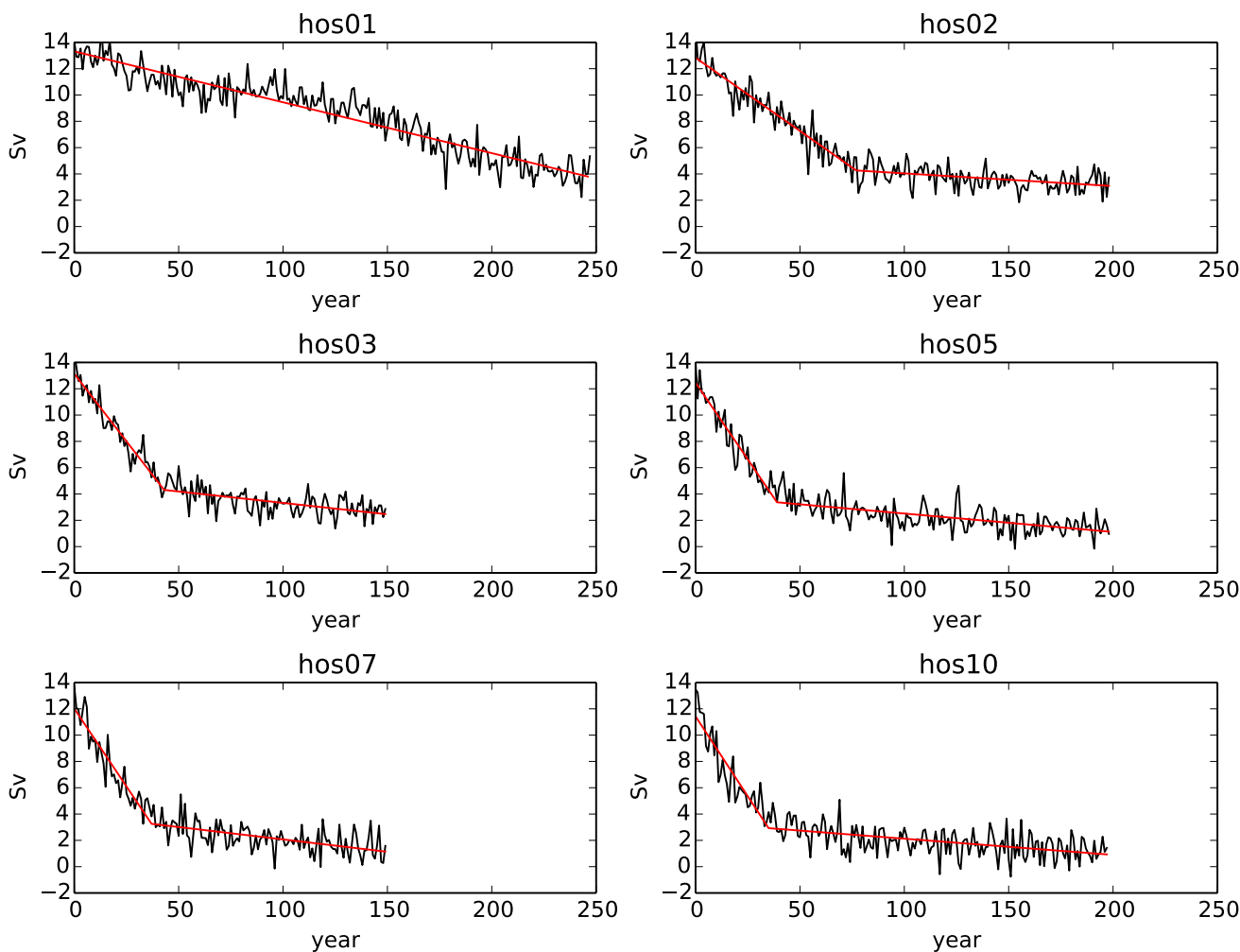


Fig. 11 AMOC timeseries (black) with best fit piecewise linear function (red). See Methods for description of function

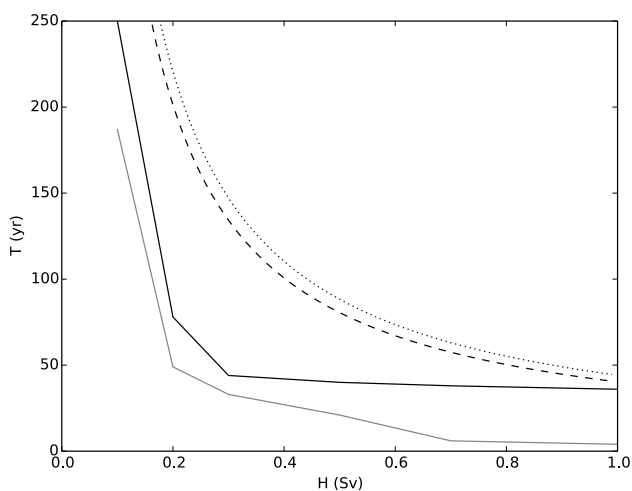


Fig. 12 Plot of T (solid black line) and T_{mld} (gray line) versus H . Also shown is the approximation from Eq. 6 for the experiments with HadGEM3-GC2 (dashed line), and with hadcm3_hos10 (dotted line)

the subpolar regions, and this salinity (and density) continues evolving after deep convection ceases as the ocean advection comes into balance with the changed surface fluxes. This time T_0 could be regarded as the time to flush salinity anomalies through the North Atlantic, so $T_0 \sim v/Q^*$, where $v \sim 10^{16} \text{ m}^3$ is the volume of interest and $Q^* \sim 10^7 \text{ m}^3/\text{s}$ is the combined volume transport from the AMOC and gyre circulations. This gives $T_0 \sim 10^9 \text{ s}$ which is a few decades and is consistent with the values of T_0 found.

We can relate the timescale of AMOC decrease to the rate of salinity change using the definition

$$\begin{aligned} \frac{\Delta Q}{T} &= \left\langle \frac{dQ}{dt} \right\rangle \\ &= \lambda \left\langle \frac{dS}{dt} \right\rangle \end{aligned}$$

where $\langle a \rangle = \int_0^T a dt/T$ is the time mean value over the first T years, $\lambda = dQ/dS$ is the relationship between the AMOC

strength Q and the salinity change, and ΔQ is the change in AMOC strength. Then

$$\frac{1}{T} = \frac{\lambda}{\Delta Q} \left\langle \frac{dS}{dt} \right\rangle \tag{5}$$

Hence the time of decline is dependent on the initial and final AMOC strengths, the magnitude of AMOC response to salinity changes, and the time mean of the salinity budget itself. Since all experiments here have approximately the same value of λ (see Fig. 2) and ΔQ , we can regard the inverse timescale as being proportional to the time mean salinity budget over the time T of the AMOC decrease.

$\langle dS/dt \rangle$ can be split into the time means of the different components of the salinity budget (Eq. 1). The time mean of each term over the first T years is shown in Fig. 13a, with the sum related to T through Eq. 5. Obviously the salinification from hosing $-F_H$ is proportional to the hosing flux H . For small values of the hosing H there is little contribution from advective fluxes to the net average change in salinity $\langle dS/dt \rangle$ whereas for large values of H there are large changes in advective fluxes which partially compensate for the greater hosing. The reason for this can be seen from Fig. 3. In all cases the anomalous advective fluxes start at zero and increase to $\approx F_H$, however the average value depends on how

quickly this change is achieved. If the advective fluxes were to increase linearly then the average value would be $F_H/2$, leading to $\langle dS/dt \rangle = -F_H/(2\nu)$ (neglecting the small surface flux terms). These relationships are shown using dotted lines in Fig. 13a. The advective fluxes do not generally increase linearly though: when the hosing is weak the advective terms take longer to respond, resulting in a convex shape and a smaller average value; when the hosing is strong the advective terms respond quickly and then level off, resulting in a concave shape and a larger average value.

An approximate timescale T can be obtained from Eq. 5 by assuming $\langle dS/dt \rangle = -F_H/(2\nu)$ (black dotted line in Fig. 13a) giving

$$T = \frac{2\nu|\Delta Q|}{\lambda F_H} \tag{6}$$

where ν is the volume of the region of the North Atlantic. Estimates of ΔQ and λ can be calculated from Fig. 2. These parameters, along with equivalent parameters from experiment hadcm3_hos10, are shown in Table 2, and the implied timescales plotted in Fig. 12. Although it gives an approximate fit to the timescale, there are clearly discrepancies. In particular note that Eq. 6 contradicts the arguments made previously that an infinitely large hosing would not instantaneously shut down the AMOC, and that for small, non zero hosing values the AMOC may not shut down at all. Nevertheless it gives an approximate way of assessing the timescale from large scale, potentially observable quantities.

The most problematic parameter to calculate would be λ , although it could be estimated from model experiments. In the two different models here λ was found to be of a similar value, however it is sensitive to the length of the timeseries used in the regression. For instance, a regression of the AMOC against S over the first 40 years in hadcm3_hos10 gives a value of 47 Sv/PSU. However the AMOC strength decreases little after this, despite additional freshening, so using the whole timeseries would give a value of λ approximately half this value, and hence double the timescale T . Roberts et al. (2013) showed regressions between subpolar Atlantic ocean densities and the AMOC in a range of GCMs for both variations due to internal variability and an AMOC decrease caused by increasing greenhouse gases. They found regression coefficients of 29–80 Sv m³/kg for the former and 79–119 Sv m³/kg for the latter, suggesting different values for the two scenarios. The regression coefficients in terms of

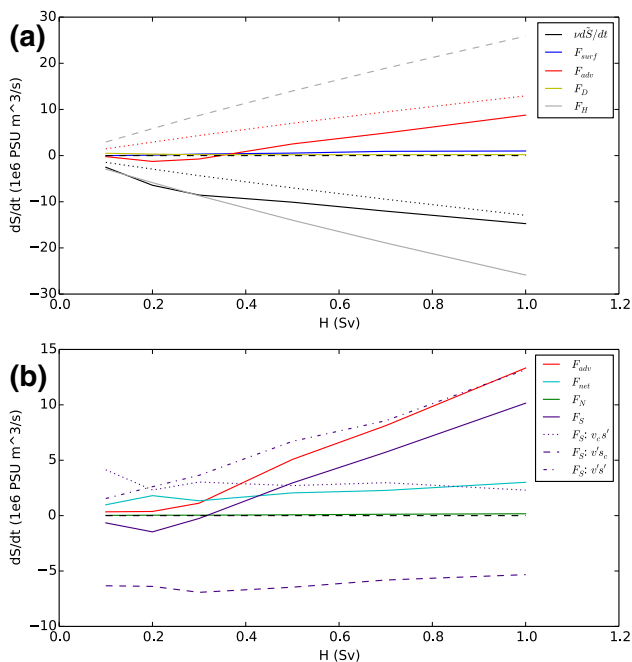


Fig. 13 Contributions to the timescale. **a** Anomalous salinity budget terms from Fig. 3 averaged over the first T years plotted against hosing H . The dashed gray line shows the line $y = F_H$, and the dotted gray and red lines show the lines $y = \pm F_H/2$. **b** Anomalous advective terms from Fig. 5 averaged over the first T years plotted against hosing H . The black horizontal dashed line shows the zero line

Table 2 Estimates of parameters from Eq. 6

Experiment	GCM	ΔQ (Sv)	λ (Sv/PSU)	ν (m ³)
hos01–hos10	HadGEM3-GC2	10.5	44	8.8×10^{16}
hadcm3_hos10	HadCM3	11.0	47	7.8×10^{16}

density in the experiments presented here are 42 and 43 Sv m^3/kg (not shown), though the region used for the volume average is different. This implies that either we need to identify a region for which λ is model and scenario independent, or that λ needs to be calculated for the scenario considered.

Discrepancies between the actual and approximate timescales are due to details of how the advection adjusts. To investigate how the advective response affects the timescale T we average the different advective components over the first T years giving different components of $\langle F_{adv} \rangle$. These are plotted against the hosing H in Fig. 13b. Advection plays little role in the salinity and AMOC reduction and hence in the timescale of weakening T for small hosing, but is an important factor in offsetting the freshening from hosing and hence delaying the AMOC reduction for large hosing. Figure 13b shows that the dominant contribution comes from changes in advection across 30°N and in particular from $F_{v,s}$, the covariance of velocity and salinity anomalies. It is this term which causes the time for AMOC reduction at high hosing rates to be much longer than would be implied by the hosing rate alone. Terms associated with changes in the throughflow transport F_{thr} , and changes from salinity alone $F_{v,s}$ have a small, positive contribution. Hence they act to lengthen the time taken for the AMOC to decrease. The contribution from velocity changes alone $F_{v,c}$ is negative and remains the same for all values of hosing since the total AMOC decrease (to ≈ 4 Sv) is the same for all experiments (see discussion in Sect. 3.3). Hence it acts to shorten the time period of AMOC decline, and has a greater relative impact when the hosing is weak.

The impacts of advective terms on the timescale could certainly be model and scenario dependent. Studies have found that applying the fresh water in different regions can result in more or less export of fresh anomalies from the region of deep water formation, and hence more or less impact on the AMOC (Smith and Gregory 2009; Weijer et al. 2012). Swingedouw et al. (2013) also showed that models differ in their export of fresh anomalies from the subpolar gyre. However we do show that results from an experiment with an independent model shows qualitatively similar advective responses.

5 Summary and conclusions

We have investigated the reduction of the AMOC when forced with additional fresh water in order to understand the processes controlling the speed of decline. We find that the rate of fresh water added is the main factor in the rate and hence time of decline, particularly when the rate is small (of order 0.1 Sv). When the rate of hosing is faster, advective feedbacks play a larger role. The advective feedbacks consist of:

- a weakening of the inter-basin sea surface height gradient, and hence the inter-basin volume transport. This imports less fresh water and hence *decelerates* the freshening and hence AMOC weakening;
- an export of fresh anomalies by the original gyre circulation which *decelerates* the freshening and hence AMOC weakening;
- less northwards import of saline water by the weakening AMOC which *accelerates* the freshening and hence AMOC weakening;
- an eastwards shift of the near surface subtropical gyre circulation which exports more of the surface fresh anomaly. This *decelerates* the freshening and hence AMOC weakening.

This final term is a feedback that has not been previously identified and which dominates the other terms when the hosing rate is large. When the hosing is large, convection shuts down more quickly resulting in the additional fresh water mainly staying in the surface layers. This fresh anomaly is exported by the gyre circulation causing a fresh, less dense anomaly in the eastern subtropics. This generates a geostrophic circulation that shifts the gyre transport eastwards, to where the water exported is fresher, and amplifies the export of the fresh anomaly. This process is found to be important in a single experiment with a second GCM, however the degree to which it is important in the weakening of the AMOC could be model dependent.

We have outlined a framework for assessing the timescale of AMOC decrease and provided estimates of the timescale based on a suite of experiments with a high resolution GCM, and a single integration of a second GCM. Although we might expect some quantitative differences from different models and different fresh water forcing scenarios given the wide range of responses of the AMOC to hosing across studies (Stouffer et al. 2006; Swingedouw et al. 2013), the similar results from this second GCM provide some measure of confidence in the qualitative robustness of the results. Concentrating on how physical mechanisms and feedbacks affect the timescale of AMOC decline provides a framework where different components can be compared across models and scenarios, leading to a greater understanding of why model responses differ. In a scenario with a more realistic distribution of future fresh water input, for example, we might expect each feedback to behave qualitatively as found in this study, although the location of fresh water might change the relative magnitudes of the response. Feedbacks, and hence controls on timescale, are also likely to be affected by warming from increased greenhouse gases. Hence this is a first step towards assessing timescales of AMOC decline and understanding whether policy-relevant conclusions can be drawn about AMOC weakening in the future. If borne out by future experiments with other models and scenarios, this gives valuable insight into the time that

may be available to adapt to committed AMOC changes in the future, or to respond through aggressive mitigation measures if it is possible to detect that an AMOC threshold has been passed.

Acknowledgements This work was supported by the Joint UK BEIS/Defra Met Office Hadley Centre Climate Programme (GA01101).

Appendix: Salinity budget derivation

Model salinity budget

The salinity (S) evolution is controlled by the equation

$$\frac{dS}{dt} = -\nabla(\mathbf{S}\mathbf{u}) + S(E - P)\delta(z - \eta) + D$$

where $\mathbf{u} = (U, V, W)$ is the three dimensional velocity, E and P are the evaporation and precipitation respectively, and $\delta(z - \eta)$ is the Dirac function that is one at the surface ($z = \eta$) and zero elsewhere (Madec 2008). D contains diffusive and sea ice terms. Integrating over a volume of the Atlantic contained by land boundaries in the x direction, by latitudes L_1 and L_2 in the y direction and from the ocean floor ($z = -H$) to the surface ($z = \eta$) we get

$$\begin{aligned} \int_{vol} \frac{dS}{dt} dx dy dz = & \int_{L_1} V S dx dz - \int_{L_2} V S dx dz - \int_{surf} W S dx dy \\ & + \int_{surf} S(E - P) dx dy + \int_{vol} D dx dy dz. \end{aligned}$$

Since the model uses a linear free surface approximation (Roulet and Madec 2000; Madec 2008) the surface for the integrals are assumed to be at $z = 0$ and hence the volume integrated over remains constant. This gives the approximation used by the model as

$$\begin{aligned} \frac{d}{dt} \int_{vol_0} S dx dy dz = & \int_{L_1} V S dx dz - \int_{L_2} V S dx dz - \int_{z=0} W S dx dy \\ & + \int_{z=0} S(E - P) dx dy + \int_{vol_0} D dx dy dz \end{aligned} \quad (7)$$

This gives the salinity budget in terms of the convergence due to lateral and vertical transports (with the vertical flux due to convergence in the free surface layer), surface fresh water fluxes (which change the salinity through implied changes in volume) and diffusive and ice terms. It is worth noting that the linear free surface has an impact on salt conservation: if the budget over the entire globe is considered, then all terms on the right hand side are zero apart from the third one. Although $\int_{z=0} W dx dy = 0$ when considering a global integral, there can be a contribution from $\int_{z=0} W S dx dy$

although this is assumed to be small since W and S at the surface are generally not correlated.

Equation 7 can then be written as

$$v \frac{d\bar{S}}{dt} = F_{adv} + F_{surf} + F_D \quad (8)$$

where v is the volume of the region, \bar{S} is the volume average salinity and F_{adv} (first 3 terms on the right hand side of Eq. 7), F_{surf} and F_D are the advective fluxes, surface fluxes and diffusive terms respectively.

Now if we write $V = \bar{V} + v$ where $\bar{V} = \int V dx dz / A$ is the section mean velocity and $A = \int dx dz$ is the section area, then we can write

$$\int V S dx dz = \bar{V} \bar{S} A + \int v S dx dz$$

where $\bar{S} = \int S dx dz / A$ is the section mean salinity. Similarly we can write

$$\int W S dx dy = \bar{W}^s \bar{S}^s A^s + \int w S dx dy$$

where $\bar{W}^s = \int W dx dy / A^s$ is the area mean of the surface vertical velocity, $A^s = \int dx dy$ and $\bar{S}^s = \int S dx dz / A^s$.

Then

$$F_{adv} = F_{thr} + F_S + F_N + F_{ws} \quad (9)$$

where

$$F_{thr} = -\bar{W}^s \bar{S}^s A^s + \bar{V}_1 \bar{S}_1 A_1 - \bar{V}_2 \bar{S}_2 A_2$$

is the advection due to the volume transport through the region having different salinities at the surface, northern and southern boundaries. We will refer to this as the throughflow component of the salinity transport.

$$F_S = \int v_1 S_1 dx dz,$$

and

$$F_N = - \int v_2 S_2 dx dz$$

are the exchanges of salt across the southern and northern boundaries respectively that are not part of the throughflow transport. The final term

$$F_{ws} = - \int w S dx dy$$

is the covariance of vertical velocities and salinities. This term is small, but non-zero in the control, however remains constant throughout the hosing experiments. Hence the contribution to the salinity budget in Eq. 2 is negligible and the term is not included.

Advection decomposition

The advective terms in F_S can be decomposed further in order to elucidate mechanisms. Note that although F_N can be decomposed in the same way, we do not do this because F_N is found to be small. One way of doing the decomposition is geometrically into zonal mean components and zonally varying anomalies. We write $v = v_o + v_g$ and $S = S_o + S_g$ where $a_o = \int v dx / \int dx$ so by definition $\int a_g dx = 0$. Then

$$\int v S dx dz = \int v_o S_o dx dz + \int v_g S_g dx dz \quad (10)$$

with the terms on the right often referred to as overturning (F_o) and gyre (F_g) components respectively.

Alternatively F_S can be decomposed to identify whether advection changes because of circulation or salinity changes. Here we decompose $v = v_c + v'$ and $S = S_c + S'$ where v_c and S_c are time mean components from the control experiment. Then

$$\int v S dx dz = \int v_c S_c dx dz + \int v_c S' dx dz + \int v' S_c dx dz + \int v' S' dx dz.$$

This is evaluated for both the hosing experiment and the control, and anomalies are taken with respect to time means of the control. Denoting the anomalous term with respect to the control using $\Delta \int v S dx dz$ we then have

$$\Delta \int v S dx dz = \Delta \int v_c S' dx dz + \Delta \int v' S_c dx dz + \Delta \int v' S' dx dz. \quad (11)$$

The first term is the anomalous advection solely due to changing salinities (assuming that the circulation remains the same as in the control), $F_{v_c S'}$; the second term is the anomalous advection solely due to changing circulation (assuming that the salinity remains the same as in the control), $F_{v' S_c}$; the third term contains the anomalous advection due to co-varying salinity and circulation, $F_{v' S'}$. Note that the time mean of the latter term in the control can be non-zero if salinity and velocity co-vary due to internal variability.

Numerical calculation

To get an accurate calculation of Eq. 8, terms for the surface, diffusive and ice fluxes are calculated at every timestep in the model code and output as annual means. The tendency term is calculated as the salinity difference between monthly mean salinity fields at the beginning and end of each year. This is not an exact representation of the tendency, which should be calculated with instantaneous salinity fields, however errors are found to be small. The advective term F_{adv} is calculated from the VS diagnostic where V and S are multiplied together (on the V grid) at every timestep within the

model code. Unfortunately an error in the WS diagnostic meant that this had to be calculated from monthly mean W and S fields, however we believe that this has introduced little error. No terms were calculated as residuals. The sea ice terms were found to be negligible and the sum of the remaining terms were found to largely match the tendency terms.

To calculate the decompositions of F_{adv} in Eq. 9, the monthly mean V and S fields were used. This means that F_{adv} also includes an additional term of $F_{eddy} = \langle VS \rangle - \langle V \rangle \langle S \rangle$ where $\langle \rangle$ indicates a monthly mean. Although this term is found to be important in other regions (Mecking et al. 2016), it is small across these boundaries so this term is neglected.

References

- Bakker P, Schmittner A, Lenaerts JTM, Abe-Ouchi A, Bi D, van den Broeke MR, Chan WL, Hu A, Beadling RL, Marsland SJ, Mernild SH, Saenko OA, Swingedouw D, Sullivan A, Yin J (2016) Fate of the Atlantic Meridional Overturning Circulation: strong decline under continued warming and Greenland melting. *Geophys Res Lett* 43:12,252–12,260. doi:10.1002/2016gl070457
- Boning CW, Behrens E, Biastoch A, Getzlaff K, Bamber JL (2016) Emerging impact of Greenland meltwater on deepwater formation in the North Atlantic Ocean. *Nat Geosci* 9(7):523–527. doi:10.1038/ngeo2740
- Cimatoribus A, Drijfhout S, Dijkstra H (2014) Meridional overturning circulation: stability and ocean feedbacks in a box model. *Clim Dyn* 42(1–2):311–328. doi:10.1007/s00382-012-1576-9
- Clement AC, Peterson LC (2008) Mechanisms of abrupt climate change of the last glacial period. *Rev Geophys* 46(4):RG4002. doi:10.1029/2006rg000204
- den Toom M, Dijkstra HA, Weijer W, Hecht MW, Maltrud ME, van Sebille E (2014) Response of a strongly Eddy global ocean to North Atlantic freshwater perturbations. *J Phys Oceanogr* 44(2):464–481. doi:10.1175/jpo-d-12-0155.1
- de Vries P, Weber SL (2005) The Atlantic freshwater budget as a diagnostic for the existence of a stable shut down of the Meridional Overturning Circulation. *Geophys Res Lett*. doi:10.1029/2004GL021450
- Driesschaert E, Fichefet T, Goosse H, Huybrechts P, Janssens I, Mouchet A, Munhoven G, Brovkin V, Weber SL (2007) Modeling the influence of Greenland ice sheet melting on the Atlantic meridional overturning circulation during the next millennia. *Geophys Res Lett* 34(10):L10707. doi:10.1029/2007gl029516
- Gent PR, McWilliams JC (1990) Isopycnal mixing in ocean circulation models. *J Phys Oceanogr* 20(1):150–155
- Gill AE (1982) *Atmosphere-ocean dynamics*. International Geophysics Series, Academic, San Francisco. doi:10.1002/qj.49711046322
- Gordon C, Cooper C, Senior CA, Banks H, Gregory JM, Johns TC, Mitchell JFB, Wood RA (2000) The simulation of SST, sea ice extents and ocean heat transports in a version of the Hadley Centre coupled model without flux adjustments. *Clim Dyn* 16:147–168
- Gregory JM, Saenko OA, Weaver AJ (2003) The role of the Atlantic freshwater balance in the hysteresis of the meridional overturning circulation. *Clim Dyn* 21(7–8):707–717. doi:10.1007/s00382-003-0359-8
- Hawkins E, Smith RS, Allison LC, Gregory JM, Woollings TJ, Pohlmann H, de Cuevas B (2011) Bistability of the Atlantic overturning circulation in a global climate model and links to ocean freshwater transport. *Geophys Res Lett*. doi:10.1029/2011GL047208

- Hofmann M, Rahmstorf S (2009) On the stability of the Atlantic meridional overturning circulation. *Proc Natl Acad Sci* 106(49):20584–20589. doi:[10.1073/pnas.0909146106](https://doi.org/10.1073/pnas.0909146106)
- Hu A, Meehl GA, Han W, Yin J (2011) Effect of the potential melting of the Greenland Ice Sheet on the Meridional Overturning Circulation and global climate in the future. *Deep Sea Res Part II Top Stud Oceanogr* 58(17–18):1914–1926. doi:[10.1016/j.dsr2.2010.10.069](https://doi.org/10.1016/j.dsr2.2010.10.069)
- Huang RX, Schmitt RW (1993) The GoldsbroughStommel circulation of the World Oceans. *J Phys Oceanogr* 23(6):1277–1284. doi:[10.1175/1520-0485\(1993\)023%3C1277:tgcotw%3E2.0.co;2](https://doi.org/10.1175/1520-0485(1993)023%3C1277:tgcotw%3E2.0.co;2)
- Jackson LC (2013) Shutdown and recovery of the AMOC in a coupled global climate model: the role of the advective feedback. *Geophys Res Lett* 40(6):1182–1188. doi:[10.1002/grl.50289](https://doi.org/10.1002/grl.50289)
- Jackson LC, Smith RS, Wood RA (2016) Ocean and atmosphere feedbacks affecting AMOC hysteresis in a GCM. *Clim Dyn*. doi:[10.1007/s00382-016-3336-8](https://doi.org/10.1007/s00382-016-3336-8)
- Liu W, Liu Z, Brady EC (2013) Why is the AMOC monostable in coupled general circulation models? *J Clim* 27(6):2427–2443. doi:[10.1175/jcli-d-13-00264.1](https://doi.org/10.1175/jcli-d-13-00264.1)
- Liu W, Xie SP, Liu Z, Zhu J (2017) Overlooked possibility of a collapsed Atlantic Meridional overturning circulation in warming climate. *Sci Adv* 3(1):e1601666. doi:[10.1126/sciadv.1601666](https://doi.org/10.1126/sciadv.1601666)
- Madec G (2008) NEMO ocean engine. Institut Pierre-Simon Laplace, France
- Manabe BS, Stouffer RJ (1999) Are two modes of thermohaline circulation stable? *Tellus A* 51(3):400–411. doi:[10.1034/j.1600-0870.1999.t01-3-00005.x](https://doi.org/10.1034/j.1600-0870.1999.t01-3-00005.x)
- Marotzke J, Willebrand J (1991) Multiple equilibria of the global thermohaline circulation. *J Phys Oceanogr* 21(9):1372–1385. doi:[10.1175/1520-0485\(1991\)021%3C1372:meotgt%3E2.0.co;2](https://doi.org/10.1175/1520-0485(1991)021%3C1372:meotgt%3E2.0.co;2)
- McCarthy GD, Smeed DA, Johns WE, Frajka-Williams E, Moat BI, Rayner D, Baringer MO, Meinen CS, Collins J, Bryden HL (2015) Measuring the Atlantic meridional overturning circulation at 26N. *Progress Oceanogr* 130:91–111. doi:[10.1016/j.pocean.2014.10.006](https://doi.org/10.1016/j.pocean.2014.10.006)
- McManus JF, Francois R, Gherardi JM, Keigwin LD, Brown-Leger S (2004) Collapse and rapid resumption of Atlantic meridional circulation linked to deglacial climate changes. *Nature* 428(6985):834–837. doi:[10.1038/nature02494](https://doi.org/10.1038/nature02494)
- Mecking JV, Drijfhout SS, Jackson LC, Graham T (2016) Stable AMOC off state in an eddy-permitting coupled climate model. *Clim Dyn* 47(7–8):2455. doi:[10.1007/s00382-016-2975-0](https://doi.org/10.1007/s00382-016-2975-0)
- Megann A, Storkey D, Aksenov Y, Alderson S, Calvert D, Graham T, Hyder P, Siddorn J, Sinha B (2014) GO5.0: the joint NERCMet Office NEMO global ocean model for use in coupled and forced applications. *Geosci Model Dev* 7(3):1069–1092. doi:[10.5194/gmd-7-1069-2014](https://doi.org/10.5194/gmd-7-1069-2014)
- Rahmstorf S (1996) On the freshwater forcing and transport of the Atlantic Thermohaline Circulation. *Clim Dyn* 12:799–811. doi:[10.1007/s003820050144](https://doi.org/10.1007/s003820050144)
- Rahmstorf S (2002) Ocean circulation and climate during the past 120,000 years. *Nature* 419(6903):207–214. doi:[10.1038/nature01090](https://doi.org/10.1038/nature01090)
- Rahmstorf S, Crucifix M, Ganopolski A, Goosse H, Kamenkovich I, Knutti R, Lohmann G, Marsh R, Mysak LA, Wang Z et al (2005) Thermohaline circulation hysteresis: a model intercomparison. *Geophys Res Lett*. doi:[10.1029/2005GL023655](https://doi.org/10.1029/2005GL023655)
- Reintges A, Martin T, Latif M, Keenlyside N (2016) Uncertainty in twenty-first century projections of the Atlantic Meridional Overturning Circulation in CMIP3 and CMIP5 models. *Clim Dyn*. doi:[10.1007/s00382-016-3180-x](https://doi.org/10.1007/s00382-016-3180-x)
- Roberts CD, Garry FK, Jackson LC (2013) A multimodel study of sea surface temperature and subsurface density fingerprints of the Atlantic meridional overturning circulation. *J Clim* 26(22):9155–9174. doi:[10.1175/jcli-d-12-00762.1](https://doi.org/10.1175/jcli-d-12-00762.1)
- Roberts CD, Jackson L, McNeill D (2014) Is the 2004–2012 reduction of the Atlantic meridional overturning circulation significant? *Geophys Res Lett* 41(9):3204–3210. doi:[10.1002/2014gl059473](https://doi.org/10.1002/2014gl059473)
- Roulet G, Madec G (2000) Salt conservation, free surface, and varying levels: A new formulation for ocean general circulation models. *J Geophys Res* 105(C10):23927–23942. doi:[10.1029/2000jc900089](https://doi.org/10.1029/2000jc900089)
- Sgubin G, Swingedouw D, Drijfhout S, Hagemann S, Robertson E (2015) Multimodel analysis on the response of the AMOC under an increase of radiative forcing and its symmetrical reversal. *Clim Dyn* 45:1429–1450. doi:[10.1007/s00382-014-2391-2](https://doi.org/10.1007/s00382-014-2391-2)
- Smith RS, Gregory JM (2009) A study of the sensitivity of ocean overturning circulation and climate to freshwater input in different regions of the North Atlantic. *Geophys Res Lett* 36(15):L15701. doi:[10.1029/2009gl038607](https://doi.org/10.1029/2009gl038607)
- Spence P, Saenko OA, Sijp W, England MH (2012) North Atlantic climate response to Lake Agassiz drainage at coarse and ocean Eddy-permitting resolutions. *J Clim* 26(8):2651–2667. doi:[10.1175/jcli-d-11-00683.1](https://doi.org/10.1175/jcli-d-11-00683.1)
- Stouffer RJ, Yin J, Gregory JM, Dixon KW, Spelman MJ, Hurlin W, Weaver AJ, Eby M, Flato GM, Hasumi H, Hu A, Jungclaus JH, Kamenkovich IV, Levermann A, Montoya M, Murakami S, Nawrath S, Oka A, Peltier WR, Robitaille DY, Sokolov A, Vettoretti G, Weber SL (2006) Investigating the causes of the response of the thermohaline circulation to past and future climate changes. *J Clim*. doi:[10.1175/JCLI3689.1](https://doi.org/10.1175/JCLI3689.1)
- Straneo F (2006) On the connection between dense water formation, overturning, and poleward heat transport in a convective basin. *J Phys Oceanogr* 36(9):1822–1840. doi:[10.1175/jpo2932.1](https://doi.org/10.1175/jpo2932.1)
- Swingedouw D, Braconnot P, Delecluse P, Guilyardi E, Marti O (2007) Quantifying the AMOC feedbacks during a 2CO₂ stabilization experiment with land-ice melting. *Clim Dyn* 29(5):521–534. doi:[10.1007/s00382-007-0250-0](https://doi.org/10.1007/s00382-007-0250-0)
- Swingedouw D, Rodehacke C, Behrens E, Menary M, Olsen S, Gao Y, Mikolajewicz U, Mignot J, Biastoch A (2013) Decadal fingerprints of freshwater discharge around Greenland in a multimodel ensemble. *Clim Dyn* 41(3–4):695–720. doi:[10.1007/s00382-012-1479-9](https://doi.org/10.1007/s00382-012-1479-9)
- Swingedouw D, Rodehacke C, Olsen S, Menary M, Gao Y, Mikolajewicz U, Mignot J (2015) On the reduced sensitivity of the Atlantic overturning to Greenland ice sheet melting in projections: a multimodel assessment. *Clim Dyn* 44(11–12):3261–3279. doi:[10.1007/s00382-014-2270-x](https://doi.org/10.1007/s00382-014-2270-x)
- Thorpe RB, Gregory JM, Johns TC, Wood RA, Mitchell JFB (2001) Mechanisms determining the Atlantic thermohaline circulation response to Greenhouse gas forcing in a non-flux-adjusted coupled climate model. *J Clim* 14:3102–3116
- Valdes P (2011) Built for stability. *Nat Geosci* 4(7):414–416. doi:[10.1038/ngeo1200](https://doi.org/10.1038/ngeo1200)
- Vallis GK (2006) Atmospheric and oceanic fluid dynamics. Cambridge University Press, Cambridge
- Vellinga M, Wu P (2004) Low latitude freshwater influence on centennial variability of the Atlantic Thermohaline Circulation. *J Clim* 17(23):4498–4511
- Weijer W, Maltrud ME, Hecht MW, Dijkstra HA, Kliphuis MA (2012) Response of the Atlantic Ocean circulation to Greenland Ice Sheet melting in a strongly-eddy ocean model. *Geophys Res Lett* 39(9):L09606. doi:[10.1029/2012gl051611](https://doi.org/10.1029/2012gl051611)
- Williams KD, Harris CM, Bodas-Salcedo A, Camp J, Comer RE, Copsey D, Fereday D, Graham T, Hill R, Hinton T, Hyder P, Ineson S, Masato G, Milton SF, Roberts MJ, Rowell DP, Sanchez C, Shelly A, Sinha B, Walters DN, West A, Woollings T, Xavier PK (2015) The met office global coupled model 2.0 (gc2) configuration. *Geosci Model Dev Discuss* 8(1):521–565. doi:[10.5194/gmdd-8-521-2015](https://doi.org/10.5194/gmdd-8-521-2015)